Supplementary Materials

Full title: Application of artificial intelligence system for screening multiple fundus diseases in Chinese primary healthcare settings: a real-world, multicenter and cross-sectional study of 4795 cases

Authors: Chufeng Gu, Yujie Wang, Yan Jiang, Feiping Xu, Shasha Wang, Rui Liu, Wen Yuan, Nurbiyimu Abudureyimu, Ying Wang, Yulan Lu, Xiaolong Li, Tao Wu, Li Dong, Yuzhong Chen, Bin Wang, Yuncheng Zhang, Wen Bin Wei, Qinghua Qiu, Zhi Zheng, Deng Liu, Jili Chen

Table of Contents

Gu C, *et al. Br J Ophthalmol* 2024; 108:1–8. doi: 10.1136/bjo-2022-322940

Table S1. Performance of ARAS in internal validation dataset

	Number of cases	Accuracy (95% CI)	Specificity (95% CI)	Sensitivity (95% CI)
Normal fundus	10749	0.816 (0.815-0.820)	0.870 (0.867-0.873)	0.773 (0.770-0.775)
Referable diabetic retinopathy	575	0.975 (0.972-0.976)	0.980 (0.978-0.981)	0.819 (0.817-0.821)
Referable hypertensive retinopathy	457	0.882 (0.881-0.885)	0.883 (0.881-0.884)	0.834 (0.832-0.839)
Glaucomatous optic neuropathy	4079	0.934 (0.932-0.935)	0.956 (0.954-0.956)	0.853 (0.852-0.856)
Pathological myopia	504	0.941 (0.939-0.942)	0.940 (0.938-0.941)	0.960 (0.958-0.961)
Retinal vein occlusion	54	0.933 (0.932-0.933)	0.933 (0.932-0.933)	0.926 (0.924-0.927)
Retinal detachment	73	0.933 (0.932-0.934)	0.933 (0.932-0.934)	0.945 (0.944-0.946)
Macula holes	32	0.955 (0.952-0.957)	0.956 (0.954-0.957)	0.938 (0.936-0.939)
Macular edema	118	0.937 (0.935-0.938)	0.938 (0.936-0.939)	0.924 (0.923-0.925)
Central serous chorioretinopathy	184	0.928 (0.927-0.930)	0.927 (0.925-0.928)	0.951 (0.950-0.952)
Epiretinal membrane	1220	0.965 (0.964-0.966)	0.964 (0.963-0.965)	0.975 (0.974-0.976)
Retinitis pigmentosa	37	0.983 (0.982-0.984)	0.983 (0.982-0.984)	0.892 (0.891-0.894)
Retina drusen	1068	0.929 (0.927-0.930)	0.926 (0.925-0.927)	0.988 (0.987-0.989)
Macular neovascularization	439	0.936 (0.935-0.937)	0.935 (0.934-0.937)	0.975 (0.974-0.976)
Geographic atrophy	40	0.973 (0.972-0.973)	0.973 (0.972-0.973)	0.925 (0.924-0.927)

For ARAS development, 115, 944 fundus images from 10 iKang Health Care centers and the Beijing Tongren Hospital between June 2018 and June 2020 were used. The dataset was then randomized into a training data set and an internal validation data set with a ratio of 5 to 1.
The above data are derived from an unpublished study.

Table S2. Performance of ARAS in external test dataset

	Number of cases	Accuracy (95% CI)	Specificity (95% CI)	Sensitivity (95% CI)
Normal fundus	170038	0.810 (0.809-0.813)	0.900 (0.898-0.902)	0.789 (0.784-0.790)
Referable diabetic retinopathy	6508	0.983 (0.981-0.984)	0.987 (0.985-0.989)	0.838 (0.836-0.845)
Referable hypertensive retinopathy	1854	0.865 (0.865-0.866)	0.865 (0.865-0.866)	0.866 (0.864-0.869)
Glaucomatous optic neuropathy	10214	0.945 (0.944-0.946)	0.949 (0.947-0.950)	0.860 (0.860-0.866)
Pathological myopia	2105	0.955 (0.954-0.956)	0.955 (0.954-0.956)	0.949 (0.948-0.951)
Retinal vein occlusion	703	0.954 (0.954-0.955)	0.954 (0.954-0.955)	0.977 (0.976-0.978)
Retinal detachment	68	0.953 (0.952-0.953)	0.953 (0.952-0.953)	0.912 (0.910-0.912)
Macula holes	235	0.951 (0.950-0.951)	0.951 (0.950-0.951)	0.877 (0.875-0.879)
Macular edema	6483	0.976 (0.975-0.977)	0.977 (0.976-0.978)	0.947 (0.946-0.948)
Central serous chorioretinopathy	92	0.926 (0.925-0.927)	0.926 (0.925-0.927)	0.967 (0.966-0.968)
Epiretinal membrane	4031	0.958 (0.957-0.959)	0.960 (0.958-0.961)	0.870 (0.868-0.872)
Retinitis pigmentosa	90	0.946 (0.945-0.947)	0.946 (0.945-0.947)	0.944 (0.943-0.945)
Retina drusen	7133	0.969 (0.967-0.969)	0.970 (0.969-0.971)	0.954 (0.953-0.956)
Macular neovascularization	1991	0.957 (0.956-0.958)	0.958 (0.957-0.959)	0.905 (0.903-0.905)
Geographic atrophy	63	0.956 (0.956-0.957)	0.956 (0.956-0.957)	0.921 (0.920-0.922)

In order to verify the performance of ARAS, 209,053 fundus images were prospectively collected (from November 2020 to February 2021) from 65 examination centers across 19 Chinese provinces.
The above data are derived from an unpublished study.

Table S3. Manufacturers and camera models used in this study

Primary healthcare settings	Manufacturer	Camera model
Linfen Community Health Service Center	Topcon	NW 300
Pengpu New Village Community Health Service Center	Topcon	NW 300
Pengpu Town Community Health Service Center	Topcon	NW 300
Bachu County People's Hospital	Topcon	NW 300
Bachu County Traditional Chinese Medicine Hospital	Syseye	RetiCam 3100
Selibuya Town Center Health Center	Syseye	RetiCam 3100

Table S4. Demographic characteristics and fundus conditions of 2528 participants in Shanghai primary healthcare settings

Variable	Total (n=2528)	Linfen Community Health Service Center (n=1349)	Pengpu New Village Community Health Service Center (n=824)	Pengpu Town Community Health Service Center (n=355)	*p*-value
Age (years)	64.0 (55.0, 70.0)	66.0 (61.0, 70.0)	64.0 (54.0, 70.0)	39.0 (30.0, 57.0)	<0.001*
Gender					<0.001*
Female	1,874 (74.1)	979 (72.6)	670 (81.3)	225 (63.4)	
Male	654 (25.9)	370 (27.4)	154 (18.7)	130 (36.6)	
Normal fundus	62 (2.5)	17 (1.3)	32 (3.9)	13 (3.7)	<0.001*
Referable diabetic retinopathy	211 (8.3)	100 (7.4)	88 (10.7)	23 (6.5)	0.011*
Referable hypertensive retinopathy	3 (0.1)	2 (0.1)	1 (0.1)	0 (0)	1
Glaucomatous optic neuropathy	394 (15.6)	227 (16.8)	128 (15.5)	39 (11.0)	0.026*
Pathological myopia	471 (18.6)	286 (21.2)	155 (18.8)	30 (8.5)	<0.001*
Retinal vein occlusion	14 (0.6)	8 (0.6)	4 (0.5)	2 (0.6)	1
Retinal detachment	0 (0)	0 (0)	0 (0)	0 (0)	/
Macular holes	12 (0.5)	7 (0.5)	4 (0.5)	1 (0.3)	1
Macular edema	79 (3.1)	47 (3.5)	25 (3.0)	7 (2.0)	0.340
Central serous chorioretinopathy	6 (0.2)	6 (0.4)	0 (0)	0 (0)	0.104
Epiretinal membranes	242 (9.6)	162 (12.0)	74 (9.0)	6 (1.7)	<0.001*
Retinitis pigmentosa	2 (0.1)	0 (0)	1 (0.1)	1 (0.3)	0.111
Retinal drusen	266 (10.5)	90 (6.7)	165 (20.0)	11 (3.1)	<0.001*
Macular neovascularization	55 (2.2)	41 (3.0)	8 (1.0)	6 (1.7)	0.005*
Geographic atrophy	5 (0.2)	4 (0.3)	1 (0.1)	0 (0)	0.699

Data are presented as median (interquartile range) or n (%).

*Statistically significant.

Table S5. Demographic characteristics and fundus conditions of 2267 participants in Xinjiang primary healthcare settings

Variable	Total (n=2267)	Bachu County Traditional Chinese Medicine Hospital (n=327)	Bachu County People's Hospital (n=1636)	Selibuya Town Center Health Center (n=304)	*p*-value
Age (years)	44.0 (32.0, 56.0)	47.0 (35.0, 56.5)	45.0 (31.0, 58.0)	41.0 (32.0, 45.0)	<0.001*
Gender					0.831
Female	1,301 (57.4)	183 (56.0)	941 (57.5)	177 (58.2)	
Male	966 (42.6)	144 (44.0)	695 (42.5)	127 (41.8)	
Normal fundus	453 (20.0)	48 (14.7)	327 (20.0)	78 (25.7)	0.003*
Referable diabetic retinopathy	175 (7.7)	17 (5.2)	155 (9.5)	3 (1.0)	<0.001*
Referable hypertensive retinopathy	5 (0.2)	0 (0)	5 (0.3)	0 (0)	0.804
Glaucomatous optic neuropathy	178 (7.9)	24 (7.3)	132 (8.1)	22 (7.2)	0.825
Pathological myopia	25 (1.1)	2 (0.6)	22 (1.3)	1 (0.3)	0.253
Retinal vein occlusion	43 (1.9)	2 (0.6)	40 (2.4)	1 (0.3)	0.008*
Retinal detachment	0 (0)	0 (0)	0 (0)	0 (0)	/
Macular holes	5 (0.2)	2 (0.6)	3 (0.2)	0 (0)	0.281
Macular edema	158 (7.0)	26 (8.0)	122 (7.5)	10 (3.3)	0.024*
Central serous chorioretinopathy	1 (0.0)	0 (0)	1 (0.1)	0 (0)	1
Epiretinal membranes	76 (3.4)	9 (2.8)	63 (3.9)	4 (1.3)	0.064
Retinitis pigmentosa	14 (0.6)	1 (0.3)	10 (0.6)	3 (1.0)	0.507
Retinal drusen	27 (1.2)	3 (0.9)	23 (1.4)	1 (0.3)	0.311
Macular neovascularization	9 (0.4)	2 (0.6)	7 (0.4)	0 (0)	0.481
Geographic atrophy	0 (0)	0 (0)	0 (0)	0 (0)	/

Data are presented as median (interquartile range) or n (%).

*Statistically significant.

Figure S1. Flowchart of the overall design in this study

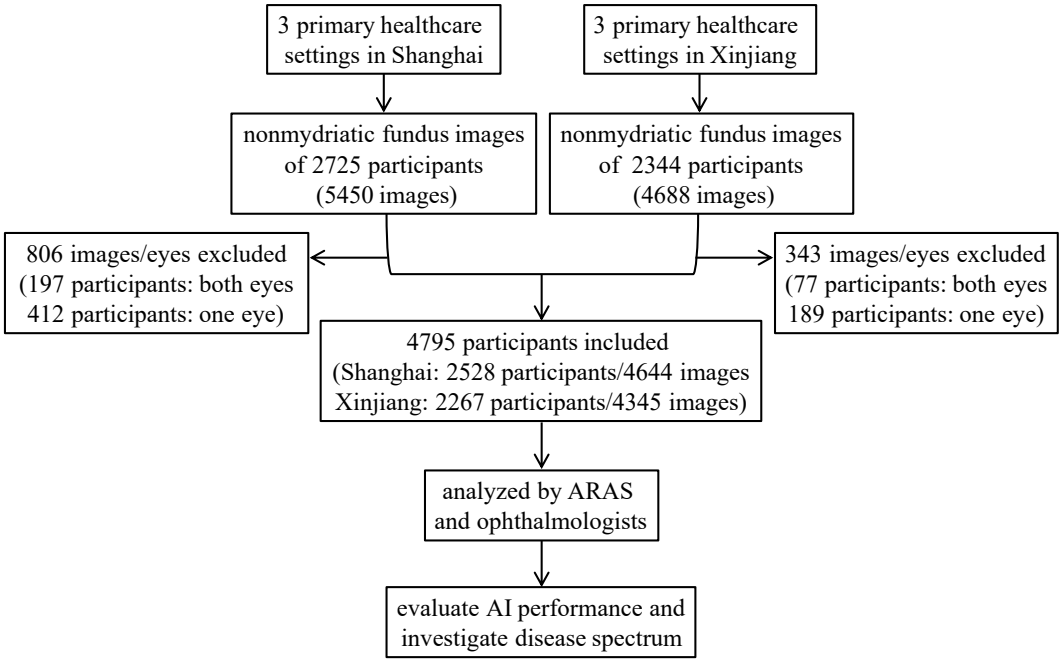

Figure S2. The overall architecture of ARAS

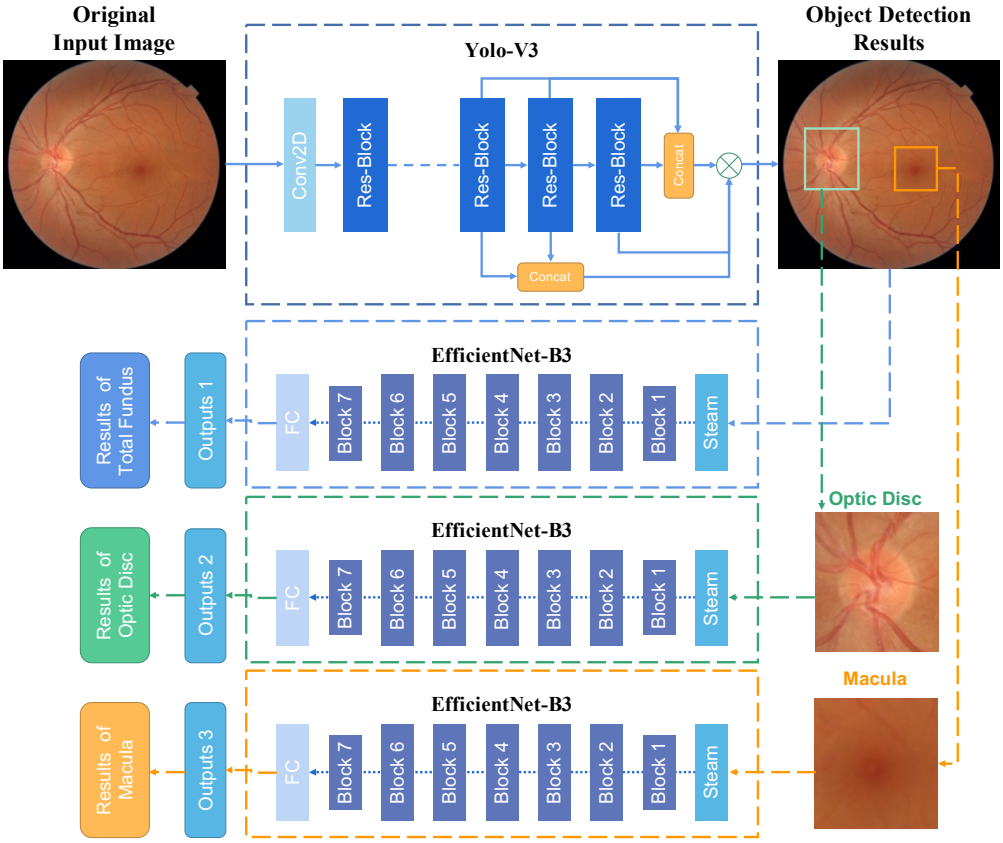

The framework consists of two AI submodules: a detection model for the macula and optic disc region and a multitask learning model for retinal disease classification.

Figure S3. Heatmap visualization of referable diabetic retinopathy

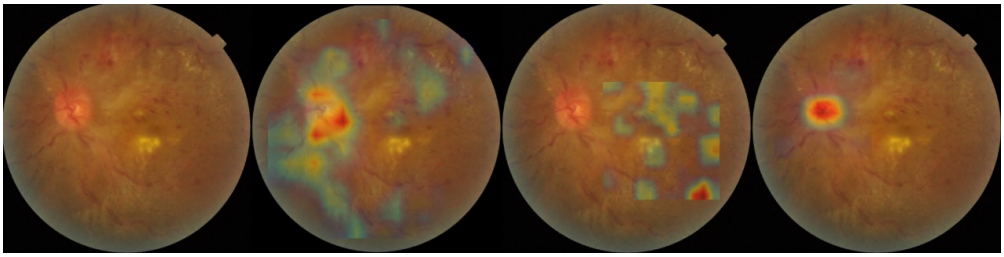

Heatmap demonstrating representative lesions, shown in original fundus image (first column), general heatmap (second column), macula heatmap (third column), and optic-disc heatmap (last column).

Figure S4. Heatmap visualization of referable hypertensive retinopathy

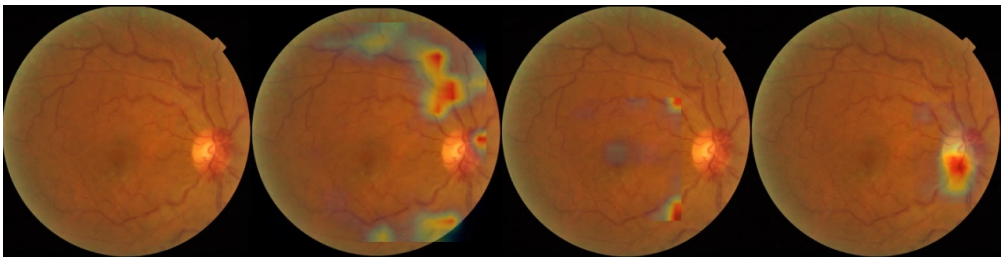

Heatmap demonstrating representative lesions, shown in original fundus image (first column), general heatmap (second column), macula heatmap (third column), and optic-disc heatmap (last column).

Figure S5. Heatmap visualization of glaucomatous optic neuropathy

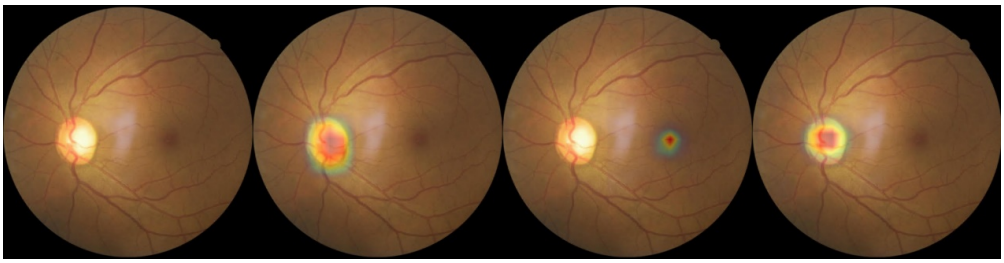

Heatmap demonstrating representative lesions, shown in original fundus image (first column), general heatmap (second column), macula heatmap (third column), and optic-disc heatmap (last column).

Figure S6. Heatmap visualization of pathological myopia

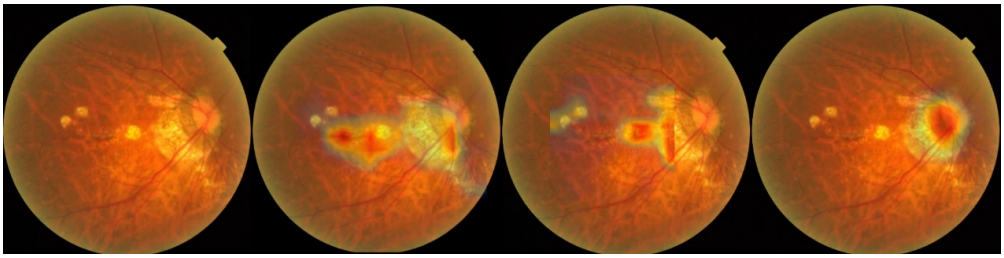

Heatmap demonstrating representative lesions, shown in original fundus image (first column), general heatmap (second column), macula heatmap (third column), and optic-disc heatmap (last column).

Figure S7. Heatmap visualization of retinal vein occlusion

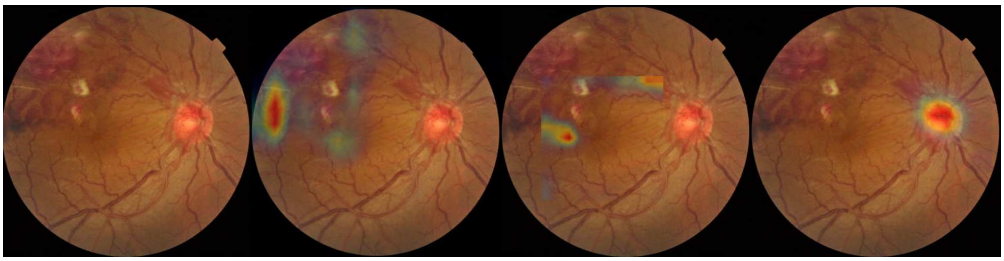

Heatmap demonstrating representative lesions, shown in original fundus image (first column), general heatmap (second column), macula heatmap (third column), and optic-disc heatmap (last column).

Figure S8. Heatmap visualization of retinal detachment

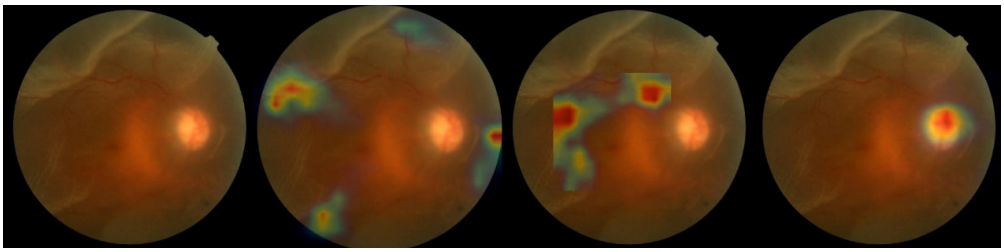

Heatmap demonstrating representative lesions, shown in original fundus image (first column), general heatmap (second column), macula heatmap (third column), and optic-disc heatmap (last column).

Figure S9. Heatmap visualization of macula holes

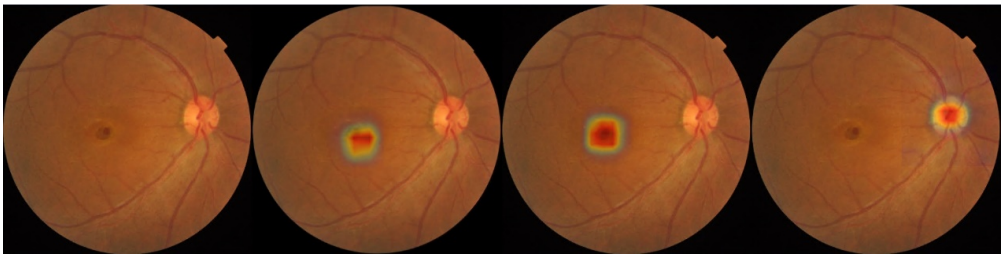

Heatmap demonstrating representative lesions, shown in original fundus image (first column), general heatmap (second column), macula heatmap (third column), and optic-disc heatmap (last column).

Figure S10. Heatmap visualization of macular edema

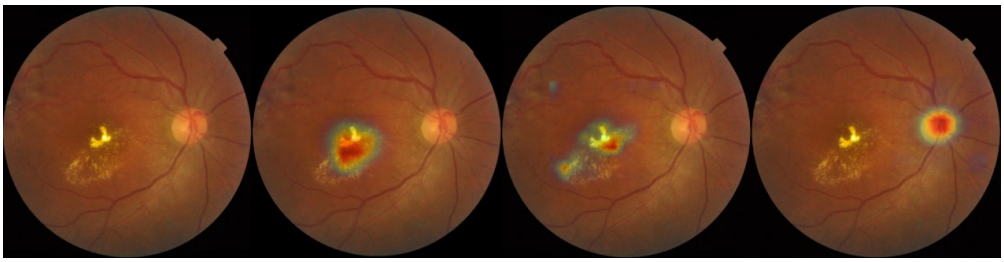

Heatmap demonstrating representative lesions, shown in original fundus image (first column), general heatmap (second column), macula heatmap (third column), and optic-disc heatmap (last column).

Figure S11. Heatmap visualization of central serous chorioretinopathy

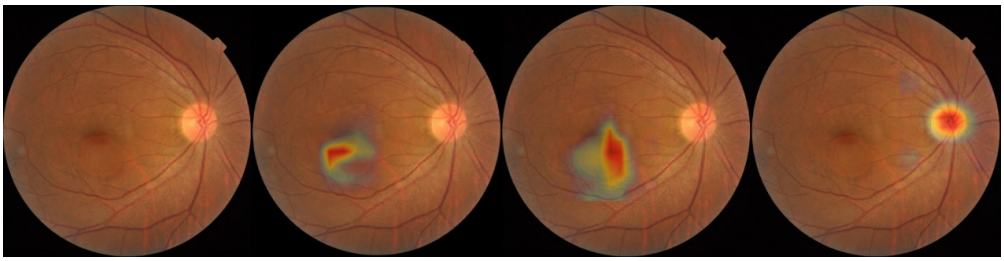

Heatmap demonstrating representative lesions, shown in original fundus image (first column), general heatmap (second column), macula heatmap (third column), and optic-disc heatmap (last column).

Figure S12. Heatmap visualization of epiretinal membrane

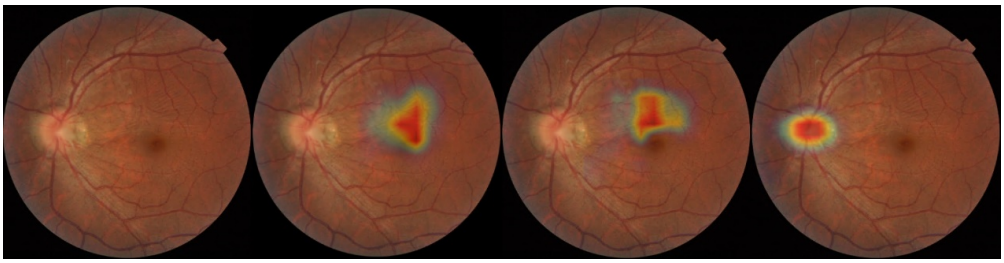

Heatmap demonstrating representative lesions, shown in original fundus image (first column), general heatmap (second column), macula heatmap (third column), and optic-disc heatmap (last column).

Figure S13. Heatmap visualization of retinitis pigmentosa

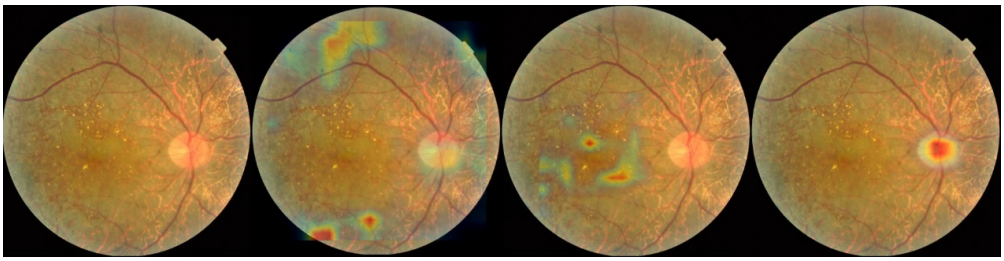

Heatmap demonstrating representative lesions, shown in original fundus image (first column), general heatmap (second column), macula heatmap (third column), and optic-disc heatmap (last column).

Figure S14. Heatmap visualization of retina drusen

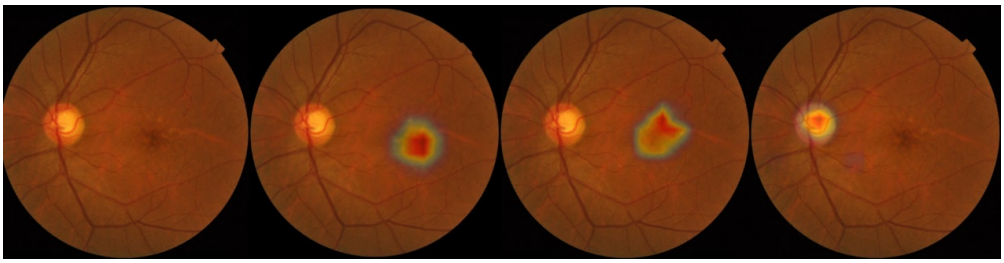

Heatmap demonstrating representative lesions, shown in original fundus image (first column), general heatmap (second column), macula heatmap (third column), and optic-disc heatmap (last column).

Figure S15. Heatmap visualization of macular neovascularization

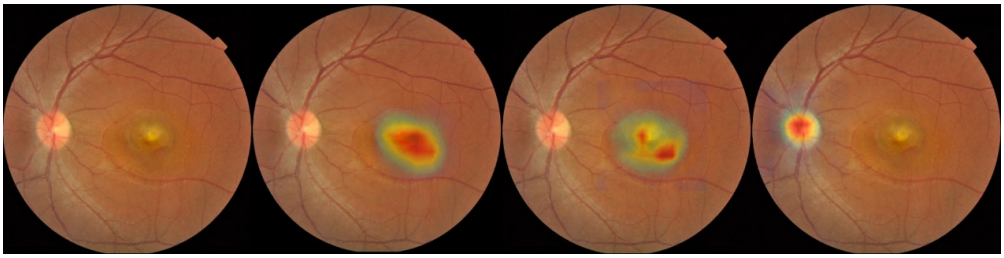

Heatmap demonstrating representative lesions, shown in original fundus image (first column), general heatmap (second column), macula heatmap (third column), and optic-disc heatmap (last column).

Figure S16. Heatmap visualization of geographic atrophy

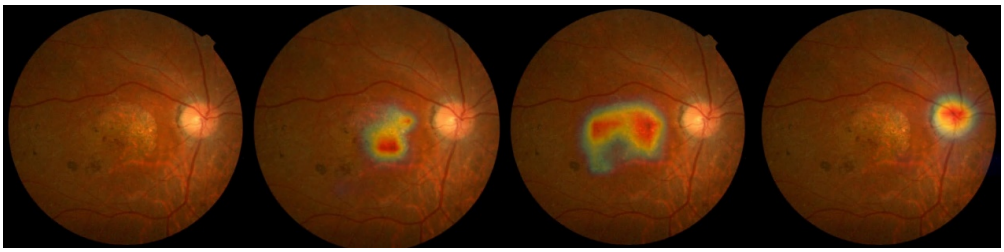

Heatmap demonstrating representative lesions, shown in original fundus image (first column), general heatmap (second column), macula heatmap (third column), and optic-disc heatmap (last column).

Figure S17. Fundus conditions of 2528 participants in Shanghai primary healthcare settings

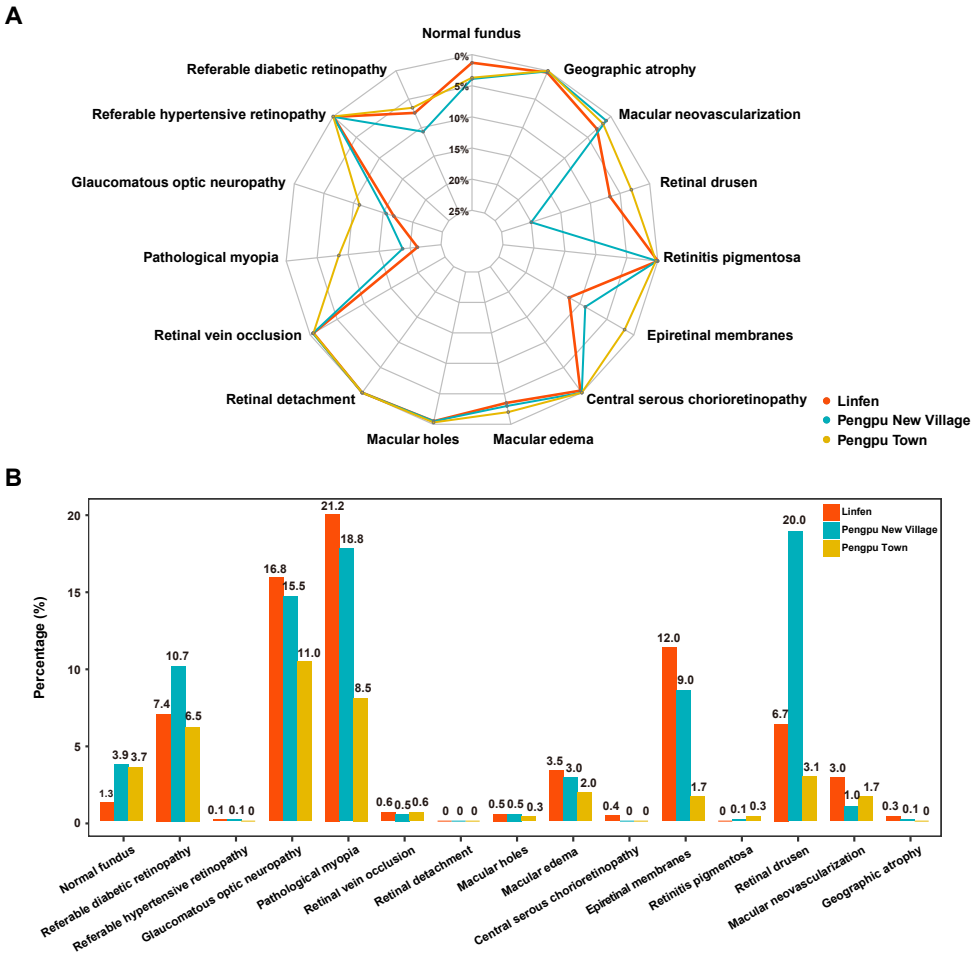

Figure S18. Fundus conditions of 2267 participants in Xinjiang primary healthcare settings